Progress In Electromagnetics Research Letters, Vol. 84, 15–21, 2019

Runge-Kutta Exponential Time Differencing Scheme for Incorporating Graphene Dispersion in the FDTD Simulations

Omar Ramadan*

Abstract—In this paper, the Runge-Kutta exponential time differencing (RK-ETD) scheme is used for incorporating Graphene dispersion in the finite difference time domain (FDTD) simulations. The Graphene dispersion is described in the gigahertz and terahertz frequency regimes by Drude model, and the stability of the implementation is studied by means of the von Neumann method combined with the Routh-Hurwitz criterion. It is shown that the presented implementation retains the standard non-dispersive FDTD time step stability constraint. In addition, the RK-ETD scheme is used for the FDTD implementation of the complex-frequency shifted perfectly matched layer (CFS-PML) to truncated open region simulation domains. A numerical example is included to validate both the stability and accuracy of the given implementation.

1. INTRODUCTION

In recent years, Graphene [1], which is considered to be a one atom two-dimensional (2-D) material, has attracted tremendous attention due to its unique electrical, optical, and mechanical properties [2]. This increases the interest in developing accurate and efficient numerical methods to simulate Graphene. In the last decade, the finite difference time domain (FDTD) method [3], one of the popular discrete time domain numerical techniques, has been successfully used in the simulation of electromagnetic wave propagation in Graphene [4–6]. In this respect, Graphene dispersion is typically characterized in the gigahertz (GHz) and terahertz (THZ) frequency regimes by a Drude model [7], and incorporated into the FDTD algorithm by a direct integration auxiliary differential equation (DI-ADE) scheme that relates the current density $\mathbf{J}$ and the electric field $\mathbf{E}$. Nevertheless, by using a similar stability analysis given in [8], it can be shown that the time step stability limit of the DI-ADE scheme of [4–6] is a function of the Graphene parameters and introduces additional stability stringent criterion other than the standard Courant-Friedrichs-Lewy (CFL) constraint and given by

$$\Delta_{t_{\max}}^{\mathcal{DI}\text{-}\mathcal{ADE}} = \frac{\Delta_{t_{\max}}^{\mathcal{CFL}}}{\sqrt{1+\mathcal{M}/\left(\Delta_{t_{\max}}^{\mathcal{CFL}}\right)^2/(4\tau)}} \tag{1}$$

where $\mathcal{M}$ and τ are related to Graphene parameters, and $\Delta_{t_{\max}}^{\mathcal{CFL}}$ is the free space CFL time step limit.

In this paper, the Runge-Kutta exponential time differencing (RK-ETD) scheme [9] is used for the FDTD implementation of Graphene dipsersion in the GHz and THz frequency ranges. By using the von Neumann method combined with the Routh-Hurwitz criterion [10], it is found that the time step stability limit of the presented implementation retains the standard non-dispersive CFL constraint. In addition, the presented RK-ETD scheme is used for the FDTD implementation of the complex-frequency shifted perfectly matched layer (CFS-PML) [11] to truncated open region simulation domains. The stability and accuracy of the presented implementation are validated through a numerical example that investigates the electromagnetic waves transmission through infinite Graphene layer.

Received 29 January 2019, Accepted 24 April 2019, Scheduled 6 May 2019

* Corresponding author: Omar Ramadan (omar.ramadan@emu.edu.tr).
The author is with the Computer Engineering Department, Eastern Mediterranean University, Famagusta, via Mersin 10, Turkey.

2. RK-ETD FDTD IMPLEMENTATION OF GRAPHENE DISPERSION

In GHz and THz frequency regimes, Graphene sheet, with a thickness of d, is typically characterized by a Drude model with effective relative permittivity of [7]

$$\varepsilon_r(\omega) = 1 + \frac{\mathcal{M}}{j\omega(j\omega\tau + 1)} \tag{2}$$

where $\mathcal{M} = \sigma_0/d\varepsilon_0$, $\sigma_0 = e^2\tau k_B T\left(\frac{\mu_c}{k_B T} + 2\ln\left(e^{-\mu_c/k_B T} + 1\right)\right)/\pi\hbar^2$, τ is the scattering time, μ_c the chemical potential, T the temperature, $-e$ the electron charge, $\hbar$ the reduced Planck's constant, and k_B the Boltzmann's constant. Then, the Maxwell's curl equations can be written in the time domain as

$$-\mu_0\frac{\partial \mathbf{H}(t)}{\partial t} = \nabla\times\mathbf{E}(t) \tag{3}$$

$$\varepsilon_0\frac{\partial \mathbf{E}(t)}{\partial t} = \nabla\times\mathbf{H}(t) - \mathbf{J}(t) \tag{4}$$

where current density $\mathbf{J}$ is governed by the following first order differential equation:

$$\frac{\partial \mathbf{J}(t)}{\partial t} = \frac{\varepsilon_0\mathcal{M}}{\tau}\mathbf{E}(t) - \frac{1}{\tau}\mathbf{J}(t) \tag{5}$$

Applying the standard leap-frog FDTD algorithm [3], the curl equations of (3) and (4) can be written in the discrete time domain as

$$-\mu_0\frac{\delta_t}{\Delta_t}\mathbf{H}^n = \widetilde{\nabla}\times\mathbf{E}\Big|^n \tag{6}$$

$$\varepsilon_0\frac{\delta_t}{\Delta_t}\mathbf{E}^{n+\frac{1}{2}} = \widetilde{\nabla}\times\mathbf{H}\Big|^{n+\frac{1}{2}} - \mu_t\mathbf{J}^{n+\frac{1}{2}} \tag{7}$$

where the fields spatial indices are not shown for the sake of brevity; Δ_t is the time step size; $\mathbf{u}^n = \mathbf{u}(n\Delta_t)$ ($\mathbf{u} = \mathbf{E}, \mathbf{H}, \mathbf{J}$); δ_t and μ_t are, respectively, the center difference and central average operators with respect to time defined as

$$\delta_t u^n = u^{n+\frac{1}{2}} - u^{n-\frac{1}{2}} \tag{8}$$

$$\mu_t u^n = \frac{u^{n+\frac{1}{2}} + u^{n-\frac{1}{2}}}{2} \tag{9}$$

and $\widetilde{\nabla}\times$ is the discrete version of $\nabla\times$ obtained by replacing the field's spatial derivatives $\partial/\partial\eta$ ($\eta = x, y, z$), by the central difference operator δ_η given by

$$\delta_\eta u^n = \frac{u^n\left(\eta + \frac{\Delta_\eta}{2}, \cdots\right) - u^n\left(\eta - \frac{\Delta_\eta}{2}, \cdots\right)}{\Delta_\eta} \tag{10}$$

where Δ_η is the space cell size in the η-direction, and finally the current density $\mathbf{J}$ is written in the discrete time domain by incorporating the RK-TDE scheme [9] into Eq. (5). To this end, multiplying Eq. (5) by $e^{t/\tau}$ and integrating over a single time step from $t = n\Delta_t$ to $t = (n+1)\Delta_t$, the following can be obtained:

$$\mathbf{J}^{n+1} = e^{-\Delta_t/\tau}\mathbf{J}^n + \frac{\varepsilon_0\mathcal{M}}{\tau}e^{-\Delta_t/\tau}\int_0^{\Delta_t} e^{t'/\tau}\mathbf{E}\left(n\Delta_t + t'\right)dt' \tag{11}$$

Applying the second-order RK-ETD scheme [9], Eq. (11) can be written as

$$\mathbf{J}^{n+1} = e^{-\Delta_t/\tau}\mathbf{J}^n + \varepsilon_0\mathcal{M}\left(1 - e^{-\Delta_t/\tau}\right)\mathbf{E}^n + \frac{\varepsilon_0\mathcal{M}\tau}{\Delta_t}\left(e^{-\Delta_t/\tau} - 1 + \frac{\Delta_t}{\tau}\right)\left(\mathbf{E}^{n+1} - \mathbf{E}^n\right) \tag{12}$$

In the following, the stability of the above RK-ETD-FDTD implementation is studied by means of von Neumann method combined with the Routh-Hurwitz criterion [10].

3. STABILITY ANALYSIS OF THE RK-ETD FDTD IMPLEMENTATION

Considering a plane wave propagating in source-free homogeneous dispersive domain and replacing the field quantities of Eqs. (6) and (7) by their complex amplitude, i.e., $\mathbf{u} \rightarrow \mathbf{u}_0$, $(\mathbf{u} = \mathbf{E}, \mathbf{H}, \mathbf{J})$ and the operators δ_η, $(\eta = x, y, z)$, δ_t and μ_t by their eigenvalues [10] as

$$\delta_\eta \rightarrow \widehat{\delta}_\eta = \frac{\mathbf{j}2\sin\left(k_\eta \Delta_\eta/2\right)}{\Delta_\eta}, \tag{13}$$

$$\delta_t \rightarrow \mathcal{Z}^{\frac{1}{2}} - \mathcal{Z}^{-\frac{1}{2}} \tag{14}$$

$$\mu_t \rightarrow \left(\mathcal{Z}^{\frac{1}{2}} + \mathcal{Z}^{-\frac{1}{2}}\right)/2 \tag{15}$$

where $\mathcal{Z} = e^{j\omega\Delta_t}$ is a complex variable corresponds to the amplification factor, and following the procedure described in [10], the stability polynomial of the presented RK-ETD implementation can be written as

$$S(\mathcal{Z}) = 4\mathcal{Z}\nu^2 + (\mathcal{Z}-1)^2\left(1 + \frac{\Delta_t}{2\varepsilon_0}\frac{\mathcal{Z}+1}{\mathcal{Z}-1}\widetilde{\sigma}\left(\mathcal{Z}\right)\right) = 0 \tag{16}$$

where $\widetilde{\sigma}(\mathcal{Z})$ is the numerical conductivity which can be obtained directly from Eq. (12) as

$$\widetilde{\sigma}(\mathcal{Z}) = \varepsilon_0\mathcal{M}\frac{\Delta_t/\tau\left(1 - e^{-\Delta_t/\tau}\right) + \left(e^{-\Delta_t/\tau} - 1 + \Delta_t/\tau\right)(\mathcal{Z}-1)}{\Delta_t/\tau\left(\mathcal{Z} - e^{-\Delta_t/\tau}\right)} \tag{17}$$

and ν is the courant number defined as

$$\nu = \frac{\Delta_t}{\Delta_{t_{\max}}^{\mathcal{CFL}}} \tag{18}$$

with $\Delta_{t_{\max}}^{\mathcal{CFL}}$ being the free space CFL time step limit given by

$$\Delta_{t_{\max}}^{\mathcal{CFL}} = \frac{\Delta}{c_0\sqrt{D}} \tag{19}$$

where $D \in \{1, 2, 3\}$ is the problem dimension, $\Delta = \Delta_x = \Delta_y = \Delta_z$ the space cell size, and $c_0 = 1/\sqrt{\varepsilon_0\mu_0}$ the speed of light. Employing the Routh-Hurwitz criterion combined with the von Neumann method [10], the stability polynomial of Eq. (16) can be written in the r-plane by substituting the transformation

$$\mathcal{Z} = \frac{r+1}{r-1} \tag{20}$$

into (16) together with (17) as

$$S(r) = \sum_{i=0}^{4} q_i r^i \tag{21}$$

where

$$\begin{aligned}
q_0 &= 4\left(1-\nu^2\right)\left(1 + e^{-\Delta_t/\tau}\right), \\
q_1 &= 4\left(\left(1-\nu^2\right) - \mathcal{M}\tau\right)\left(1 - e^{-\Delta_t/\tau}\right) + 2\mathcal{M}\Delta_t\left(1 + e^{-\Delta_t/\tau}\right), \\
q_2 &= 4\nu^2\left(1 + e^{-\Delta_t/\tau}\right) + 2\mathcal{M}\Delta_t\left(1 - e^{-\Delta_t/\tau}\right), \\
q_3 &= 4\nu^2\left(1 - e^{-\Delta_t/\tau}\right).
\end{aligned}$$

In this transformation, the exterior of the unit circle in the $\mathcal{Z}$-plane is mapped onto the right half of the r-plane. Therefore, if $S(r)$ has no roots in the right half of the r-plane, then $S(\mathcal{Z})$ will not have any root outside the unit circle of the $\mathcal{Z}$-plane. It must be noted that $S(r)$ polynomial will not have roots in the right half of the r-plane if all entries of the first column of the Routh table, which can be

constructed from $S(r)$, are non-negative [10]. To this end, the Routh table can be constructed from Eq. (21) as [10]

$$\begin{array}{ll} q_3 & q_1 \\ q_2 & q_0 \\ c_{3,0} = q_2 - \frac{q_3 q_0}{q_2} & 0 \\ q_0 & 0 \end{array} \tag{22}$$

Forcing all entries of the first column of Eq. (22) to be non-negative, and considering the inequality

$$q_0 = 4\left(1-\nu^2\right)\left(1+e^{-\Delta_t/\tau}\right) \geq 0 \tag{23}$$

and using Eq. (18), the time step limit can be obtained as

$$\Delta_{t_{\max}} = \Delta_{t_{\max}}^{\mathcal{CFL}} \tag{24}$$

Hence, the presented RK-ETD FDTD implementation of Graphene dispersion maintains the standard non-dispersive CFL limit.

4. RK-ETD FDTD IMPLEMENTATION OF THE CFS-PML MESH TRUNCATING TECHNIQUE

To model open region problems using the FDTD algorithm, efficient and reliable mesh truncating techniques are required to truncate the computational domain. In this paper, the RK-ETD scheme is employed into the FDTD implementation of the CFS-PML [11], which is considered to be one on the most effective FDTD mesh truncating techniques. Based on the formulations of [11], the space derivatives of the field equations in the CFS-PML regions at the domain boundaries are modified as

$$\frac{\partial u}{\partial \eta} \rightarrow \frac{1}{S_\eta}\frac{\partial u}{\partial \eta} \tag{25}$$

where S_η, $\eta = x, y, z$, is the complex stretched coordinate metric given by

$$S_\eta = \kappa_\eta + \frac{\sigma_\eta}{\alpha_\eta + j\omega\varepsilon_o} \tag{26}$$

where σ_η, κ_η, and α_η are one-dimensional real positive metrics designed inside the CFS-PML region to absorb the outgoing electromagnetic waves with minimal reflections and given by the following graded polynomials:

$$\sigma_\eta = \sigma_\eta^{\max}\left(\frac{\eta}{\mathcal{D}}\right)^m \tag{27}$$

$$\kappa_\eta = 1 + \left(\kappa_\eta^{\max} - 1\right)\left(\frac{\eta}{\mathcal{D}}\right)^m \tag{28}$$

$$\alpha_\eta = \alpha_\eta^{\max}\left(\frac{\mathcal{D}-\eta}{\mathcal{D}}\right)^{m_\alpha} \tag{29}$$

where η is the depth in the CFS-PML; $\mathcal{D}$ is the CFS-PML thickness; and m_α and m are the graded polynomial orders. Noting the identity

$$\frac{1}{S_\eta} = \frac{1}{\kappa_\eta} - \frac{\sigma_\eta}{\kappa_\eta}\frac{1}{\kappa_\eta(\alpha_\eta + j\omega\varepsilon_o) + \sigma_\eta} \tag{30}$$

Equation (25) can be expressed as

$$\frac{1}{S_\eta}\frac{\partial u}{\partial \eta} = \frac{1}{\kappa_\eta}\frac{\partial u}{\partial \eta} - Q_{\eta,u} \tag{31}$$

where $Q_{\eta,u}$ is governed by the following the time domain ADE:

$$\frac{\partial}{\partial t}Q_{\eta,u} + \Gamma Q_{\eta,u} = \Omega\frac{\partial u}{\partial \eta} \tag{32}$$

where $\Omega = (\kappa_\eta \alpha_\eta + \sigma_\eta)/\kappa_\eta \varepsilon_o$ and $\Gamma = -\sigma_\eta/\kappa_\eta^2 \varepsilon_o$. Based on Eqs. (31) and (32), and considering the x-projection of Ampere's law of Eq. (4), as an example, the E_z field component can be written in the discrete form in CFS-PML region as

$$\varepsilon_0 \frac{\delta_t}{\Delta_t} E_z^{n+1/2} = \frac{1}{\kappa_x} \frac{\partial H_y}{\partial x}\bigg|^{n+1/2} - Q_{x,H_y}^{n+1/2} - \frac{1}{\kappa_y} \frac{\partial H_x}{\partial y}\bigg|^{n+1/2} + Q_{y,H_x}^{n+1/2} - \mu_t J_z^{n+\frac{1}{2}} \tag{33}$$

where $Q_{\eta,u}^{n+1/2}$, for $(\eta, u) = (x, H_y)$ or (y, H_x), is obtained by discretizing Eq. (32) using the RK-ETD scheme. For example, $Q_{x,H_y}^{n+1/2}$ can be obtained by multiplying Eq. (32) by $e^{\Gamma \Delta_t}$ and integrating over a single time step from $t = (n - 1/2)\Delta_t$ to $t = (n + 1/2)\Delta_t$, and applying the second-order RK-ETD scheme [9], the following can be obtained:

$$\begin{aligned} Q_{x,H_y}^{n+1/2} \;=\; & e^{-\Delta_t \Gamma} Q_{x,H_y}^{n-1/2} + \frac{\Omega}{\Gamma}\left(1 - e^{-\Gamma \Delta_t}\right) \frac{\partial H_y}{\partial x}\bigg|^{n-1/2} \\ & + \frac{\Omega}{\Gamma^2 \Delta_t}\left(e^{-\Gamma \Delta_t} - 1 + \Gamma^2 \Delta_t\right)\left(\frac{\partial H_y}{\partial x}\bigg|^{n+1/2} - \frac{\partial H_y}{\partial x}\bigg|^{n-1/2}\right) \end{aligned} \tag{34}$$

Similar equations can be obtained for the other field equations.

5. SIMULATION STUDY

To study the stability and accuracy of the presented RK-ETD FDTD implementation, consider the problem of a plane-wave, with the fields of E_z and H_y propagating in the x-direction, normally incident on an infinite free-standing Graphene sheet in free space. A computational domain, with a size of 4000Δ and terminated by additional 10-cell thick CFS-PML, is considered in this study. The FDTD spatial cell size is set to $\Delta = 20\,\text{nm}$, and the parameters for CFS-PML graded polynomials of Eqs. (27)–(29) are taken as $\sigma_x^{\max} = 0.8(m+1)/(\Delta\sqrt{\mu_0/\varepsilon_0})$, $\alpha_x^{\max} = 0.05$, $\kappa_x^{\max} = 1$, $m = 3$, and $m_\alpha = 1$. The Graphene layer occupies one FDTD cell located at node 2000, with the parameters of $T = 300\,\text{Kelvin}$, $\mu_c = 0.5\,\text{eV}$, $\tau = 0.5\,\text{ps}$, and $d = \Delta = 20\,\text{nm}$. The time dependence of the excitation function is given by $g(t) = \exp(-4\pi(t - t_c)^2/t_d^2)$, where $t_d = 100\Delta_t$ and $t_c = 3t_d$. The source point (**S**) is located at node 10, and the observation point (**O**) is placed 20 FDTD cells away from the back of the Graphene layer at node 2020. Fig. 1 shows the simulation domain geometry. The simulation is performed for 200,000 time steps.

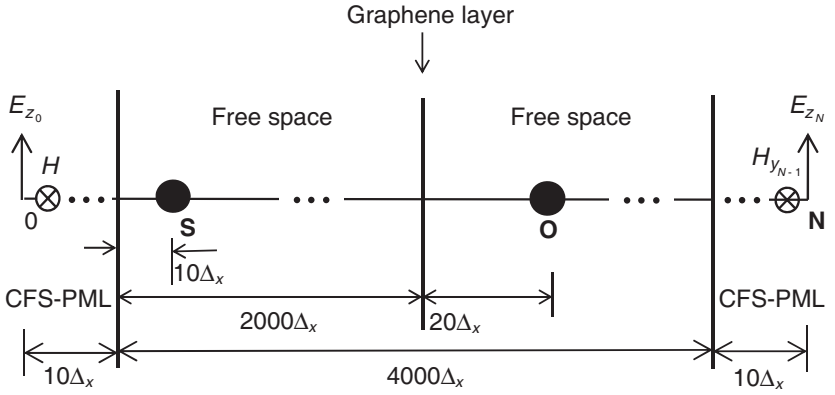

Figure 1. Simulation domain geometry, where **S** and **O** are the source and observation points, respectively.

The stability of the implementation is studied first. Fig. 2(a) shows the electric field recorded at the observation point, $E_z^{gr}(2020\Delta)$ computed with a time step set to $\Delta_t = \Delta_{t\,\max}^{\mathcal{CFL}} = 66.712 \times 10^{-18}\,\text{s}$ as obtained with the presented RK-ETD FDTD scheme where no instability occurs over the whole

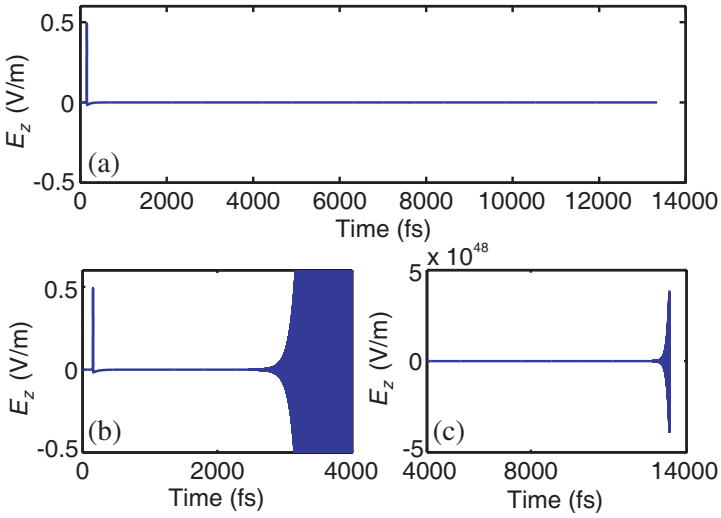

Figure 2. Electric field recorded at node 2020 ($E_z^{gr}(2020\Delta)$) as obtained with $\Delta_t = \Delta_{t_{\max}}^{\mathcal{CFL}}$ for the presented RK-ETD formulation (a), and the DI-ADE formulation of [5] in the early time (b) and in the late time (c).

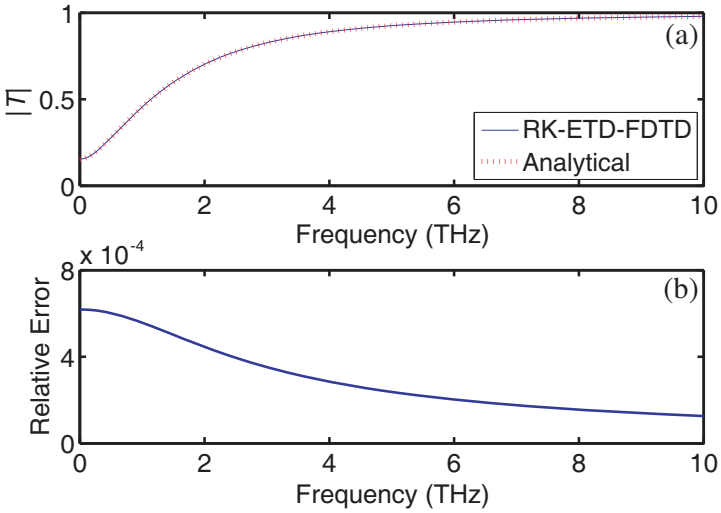

Figure 3. (a) Transmission coefficient magnitude for a normally incident plane wave through the Graphene layer obtained by the presented RK-ETD FDTD implementation and the analytical approach. (b) The relative error between the RK-ETD FDTD simulation and analytical result.

period of time. For the purpose of comparison, Figs. 2(b) and (c) show the field obtained by the DI-ADE scheme [5] with $\Delta_t = \Delta_{t\,\max}^{\mathcal{CFL}}$ in the early time and in the late time, respectively. It can be seen that the field starts to be unstable in the early time and increases without bound in the late time. Therefore, the DI-ADE implementation of [5] does not maintain the standard CFL constraint. The accuracy of the implementation is also investigated by computing the transmission coefficient of the Graphene layer. For this case, an auxiliary simulation that uses the same configuration but replaces the Graphene sheet by a vacuum layer is performed to record the reference field at the observation point, i.e., $E_z^{air}(2020\Delta)$. Then, the time-domain data of E_z^{gr} and E_z^{air} are Fourier transformed, and their ratio determines the transmission coefficient. Fig. 3(a) shows the transmission coefficient magnitude as a function of frequency as calculated by using the presented RK-ETD implementation ($|\mathcal{T}_{\mathcal{RK}\text{-}\mathcal{ETD}}|$) and the analytical transmission ($|\mathcal{T}_a|$) approach [12]. Fig. 3(b) shows the relative error between the two

solutions and computed by $|\left(\mathcal{T}_a - \mathcal{T}_{\mathcal{RK}-\mathcal{ETD}}\right)/\mathcal{T}_a|$. Clearly, strong agreement can be observed between the RK-ETD FDTD and the analytical results, where a relative error less than 0.08% is achieved over the frequency range of interest, and this confirms the accuracy of the presented RK-ETD FDTD implementation.

6. CONCLUSION

In this paper, the RK-ETD scheme is used for incorporating the Drude dispersion of Graphene into the FDTD simulations in the THz frequency range. The implementation maintains the CFL stability limit of the standard non-dispersive FDTD algorithm. The RK-ETD scheme is also employed in the FDTD implementation of the CFS-PML mesh truncation technique. A numerical example which investigates the electromagnetic wave transmission through Graphene layer confirms both the stability and accuracy of the given implementations.

REFERENCES

1. Geim, K. and K. S. Novoselov, "The rise of Graphene," *Nat. Mater.*, Vol. 6, No. 3, 183–191, 2007.
2. Novoselov, K. S., V. I. Falko, L. Colombo, P. R. Gellert, M. G. Schwab, and K. Kim, "A roadmap for Graphene," *Nature*, Vol. 490, 192–200, 2012.
3. Taflove, A. and S. Hangess, *Computational Electrodynamics: The Finite-Difference Time-Domain Method*, 3rd Edition, Artech-House, Norwood, MA, 2005.
4. Bouzianas, D., N. Kantartzis, S. Antonopoulos, and T. Tsiboukis, "Optimal modeling of infinite Graphene sheets via a class of generalized FDTD schemes," *IEEE Trans. Magn.*, Vol. 48, No. 2, 379–382, 2012.
5. Bouzianas, G. D., N. V. Kantartzis, T. V. Yioultsis, and T. Tsiboukis, "Consistent study of Graphene structures through the direct incorporation of surface conductivity," *IEEE Trans. Magn.*, Vol. 50, No. 2, Art. No. 7003804, 2014.
6. Papadimopoulos, A. N., S. A. Amanatiadis, N. V. Kantartzis, I. T. Rekanos, T. T. Zygiridis, and T. D. Tsiboukis, "A convolutional PML scheme for the efficient modeling of Graphene structures through the ADE-FDTD technique," *IEEE Trans. Magn.*, Vol. 53, No. 6, Art. No. 7204504, 2017.
7. Sounas, L. and C. Caloz, "Gyrotropy and nonreciprocity of Graphene for microwave applications dimitrios," *IEEE Trans. Microw. Theory Tech.*, Vol. 60, No. 4, 901–914, 2012.
8. Young, J. L., A. Kittichartphayak, Y. M. Kwok, and D. Sullivan, "On the dispersion errors related to $(FD)^2TD$ type schemes," *IEEE Trans. Microw. Theory Tech.*, Vol. 43, No. 8, 1902–1909, 1995.
9. Cox, S. M. and P. C. Matthews, "Exponential time differencing for stiff systems," *J. Comput. Phys.*, Vol. 176, 430–455, 2002.
10. Pereda, J. A., L. A. Vielva, A. Vegas, and A. Prieto, "Analyzing the stability of the FDTD technique by combining the Von Neumann method with the Routh-Hurwitz criterion," *IEEE Trans. Microw. Theory Tech.*, Vol. 49, No. 2, 377–381, 2001.
11. Kuzuoglu, M. and R. Mittra, "Frequency dependence of the constitutive parameters of causal perfectly matched anisotropic absorbers," *IEEE Microw. Guided Wave Lett.*, Vol. 6, No. 12, 447–449, Dec. 1996.
12. Hanson, G. W., "Dyadic Green's functions and guided surface waves for a surface conductivity model of graphene," *J. Appl. Phys.*, Vol. 103, No. 064302, 2008.